Journal of Materials Chemistry A

Accepted Manuscript

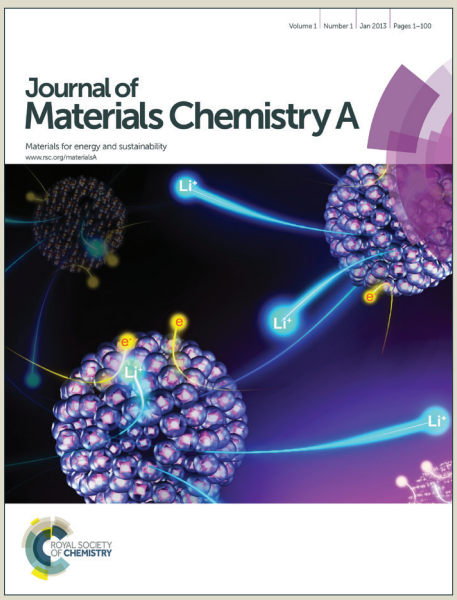

ROYAL SOCIETY OF CHEMISTRY

www.rsc.org/materialsA

Journal of Materials Chemistry A

Dynamic Article Links►

Cite this: DOI: 10.1039/c0xx00000x

PAPER

www.rsc.org/xxxxxx

Investigation into the origin of pseudocapacitive behavior of Mn_3O_4 electrodes using operando Raman spectroscopy

Lufeng Yang[a], Shuang Cheng[*a], Xu Ji[c], Yu Jiang[a], Jun Zhou[a] and Meilin Liu[*ab]

Received (in XXX, XXX) Xth XXXXXXXXX 20XX, Accepted Xth XXXXXXXXX 20XX
DOI: 10.1039/b000000x

A profound understanding of the phase changes of manganese oxides in a pseudocapacitor during cycling is vital to unrevealing the mechanism of energy storage in the material and achieving rational design of better electrode materials. Here we report our findings in probing the phase changes of a Mn_3O_4 electrode material in a pseudo-capacitor during a charging/discharging process using *in operando* Raman spectroscopy. Results indicate that accompanied with performance enhancement, the spinel Mn_3O_4 is transformed to a layered birnessite-type MnO_2 upon potential cycling and two types of processes contribute to the energy storage, the intercalation/deintercalation of Na^+ and oxidation/reduction of Mn^{2+}. After charging and discharging for ~10,000 cycles, the specific capacitance of manganese oxide is increased by almost 3 times; the maximum specific capacitance approaches 230 F g^{-1} at a cycling rate of 0.5 A g^{-1}.

Introduction

Because of their high power density and long operational life, supercapacitors are an important energy-storage device, especially for high-power, short pulse applications. They can also be integrated with batteries and fuel cells to meet a wide range of power requirements.[1, 2] As new materials are being developed to enhance the energy density of supercapacitors, their applications are broadened, becoming more attractive for emerging applications such as electrical vehicles and smart grids. Unlike electric double layer capacitors (EDLCs), which are based on accumulation of ions at the electrode/solution interface, pseudocapacitors make use of fast redox reactions on the surface or subsurface of the active electrode materials.[3-5] Among the most widely used active electrode materials,[3, 6] both conducting polymers[5, 7] and transition-metal oxides[8-10] have been developed as the electrode materials for pseudocapacitors; however, transition-metal oxides are considered more promising due to their potential to offer much higher energy densities. Manganese oxides (MnO_x) are one type of prospective candidates because of their high theoretical capacitance (>1000 F/g), environmental friendliness and natural abundance.[11-13] To date, however, most of the efforts on MnO_x based materials have been devoted to optimization of the capacities by designing superior electrode architectures, desirable crystal structures, or morphologies via complex synthesis. The underlying charge-storage mechanism of MnO_x pseudo-capacitors is still lacking. Lately, Mn_3O_4 thin films have been synthesized by a chemical bath deposition method and experienced a phase transformation into layered birnessite MnO_2 with significantly enhanced capacitance under voltammetric cycling test.[14, 15] Two reactions involved in the charge storage/release process are proposed. The spinel Mn_3O_4 was first transformed to layered birnessite MnO_2 through a complex and irreversible process, then the birnessite MnO_2 experienced an intercalation/deintercalation of cations C^+ (including protons and electrolyte cations) between the sheets during potential cycling.

$$Mn_3O_4(spinel) \xrightarrow{potential\ cycling} C_\delta MnO_2 \cdot nH_2O(birnessite) \quad (1)$$

$$C_\delta MnO_2 \cdot nH_2O \leftrightarrow MnO_2 \cdot nH_2O + \delta C^+ + \delta e^- \quad (2)$$

Nevertheless, the underlying physical processes of the structural changes and the charge storage behavior of the active electrode materials during cycling are yet to be fully understood, e.g. at what stage the transformation starts, how the transformation performs (dissolving, then growing; or crystal structure change directly). Recently, *ex-situ* X-ray diffraction was used to investigate a Mg-doped sodium birnessite-type MnO_2 in an effort to correlate cation intercalation/deintercalation with the changes in interlayer spacing.[16] Unfortunately, a progressive crystallinity loss of the material impedes further investigation of the structural evolution upon electrochemical cycling. In our recent work,[17] we have demonstrated the utility of *in operando* Raman spectroscopy to probe phase evolution of non-stoichiometric α-MnO_2 based electrode materials in a supercapacitor during a charging/discharging process. Raman data of manganese oxides with a mix-phase of α-MnO_2 and Mn_3O_4 were interpreted in a local operating environment, which allows us to monitor the relationship between the lattice vibrations of MnO_x that corresponds to specific structure and the operating condition during practical use. The effect of Mn^{2+} on

the charge storage behavior of Mn_3O_4 was proposed. The intercalation/deintercalation of Mn^{2+} induced a reversible phase change between Mn_3O_4 and MnO_2, while the irreversible part resulted in reduction of Mn_3O_4 during a long life test. Yet, the phase structure is very complex, more stable and pure single phase samples are needed to gain more insight into the energy storage mechanism of Mn_3O_4.

In this study, Mn_3O_4 thin films were deposited on carbon fiber paper using a simple electrochemical deposition procedure, followed by a heat treatment in nitrogen. Raman spectroscopy was then used to probe the structural changes of the active electrode material in a pseudocapacitor during potential cycling, to gain more understanding of the structural evolution and its effect to the charge storage mechanism of Mn_3O_4. Moreover, the energy storage process of the transformed birnessite-type MnO_2 was also examined. Additionally, the versatile strategy developed in this study may be used for the characterization of energy storage mechanism of other transition metal oxides based electrode materials.

Experimental section

2.1 Preparation of Mn_3O_4 thin film

All reagents were of analytical grade and used directly without further purification. Mn_3O_4 thin films were prepared by a simple electrochemical deposition process in a conventional three-electrode cell, followed by a heat treatment under Nitrogen flow at 400 ºC for 3 hour. In a typical synthesis procedure, pieces of carbon fiber paper (Hesen, Shanghai Electric. Co.) were dipped in concentrated sulfuric acid (98% H_2SO_4 solution) for 10 min first, then rinsed with deionized water, dried at 110 ºC for 2 h and weighted. The pre-treated carbon fiber paper (CFP) was used as working electrode. A Pt mesh of about 1.0 cm^2 and a saturated calomel electrode (SCE) connected to the cell were used as counter electrode and reference electrode, respectively. The manganese oxide film was anodic electrodeposited on the pre-treated CFP in aqueous solution of 0.01 M $Mn(NO_3)_2$ + 0.02 M NH_4NO_3 + 10% dimethyl sulfoxide (DMSO) by galvanostatic electrolysis at 0.1 mA·cm^{-2} for 30 min at 70 ºC using an electrochemical analyzer system, CHI 660E (Chenhua, Shanghai, China), then calcined in N_2 at 400 ºC for 3 h. The mass of final loaded Mn_3O_4 was weighted with a BT 25 S analytical balance (Sartorius; δ=0.01 mg) and confirmed with mass calculation by Faraday's law.

2.2 Characterization

The surface morphologies were examined by a field emission scanning electron microscope (FE–SEM, Hitachi LEO 1530). The X-ray diffraction (XRD) pattern was recorded on a Bruker D8 Advance X-ray diffractometer with Cu Ka radiation (λ= 0.15406 nm) at a gracing parallel incidence of 3 degree. *In situ* Raman test was run on a Lab RAM HR Evolution system equipped with deep-depleted thermoelectrically cooled CCD array detector, an Ar laser (wavelength=514.5nm) and long working distance 50× objective lens. Mapping tests on time of one spectrum capture in every 100 seconds were set when the three-compartment cell run cyclic voltammetry at sweep rates of 1 mV/s in a potential range of 0-1.0 V. The exploration time is 10 second with twice sweeping for one spectrum, and the size of optical hole is 100 μm.

2.3 Electrochemical measurement

The electrochemical properties of Mn_3O_4 thin film were studied by a CHI 660E workstation in a three-electrode conguration with Mn_3O_4 thin film prepared on CFP as the working electrode, and a Ag/AgCl (in saturated KCl) and a Pt mesh as the reference and counter electrodes respectively. A solution containing 1 M Na_2SO_4 served as electrolyte at room temperature. Cyclic voltammetric (CV) durability test were performed between 0 and 0.8 V vs Ag/AgCl at a scan rate of 50 mV/s.

Results and discussion

3.1 structure studies

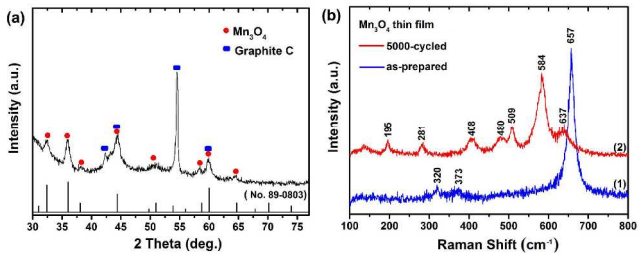

Fig. 1 (a) XRD patterns of the as-prepared sample, (b) Raman spectra of (1) the as-prepared and (2) after 5000 cycles running sample.

Fig. 1a shows the XRD patterns of as prepared samples. The peaks with higher intensity marked with blue squares all belong to graphite carbon substrate (JCPDS card no. 41-1487, Fig. 1a). And the peaks marked with red circle are in good agreement with tetragonal hausmannite Mn_3O_4 structure (JCPDS card no. 89-0803, Fig. 1a). Mn_3O_4 is known to have a normal spinel structure with tetragonal distortion elongated along the c-axis due to Jahn-Teller effect of the Mn^{3+} ion. The Mn^{3+} ions occupy the B-site (octahedral) while the Mn^{2+} ions are at the A-site (tetrahedral).[18] After durability CV test of 5000 cycles, all the peaks assigned to Mn_3O_4 disappeared and reflections at (002), (120), (204), (161), (235), (324), (544) and (611) emerged which can be recognized as layered birnessite-type MnO_2 (JCPDS card no. 23-1046, Fig. S1). This result revealed that the as-prepared Mn_3O_4 film is converted into layered birnessite MnO_2 during the electrochemical oxidation during potential cycling. Since Raman spectroscopy can be performed under *in operando* conditions and offers valuable information complementary to X-ray diffraction (XRD) for structural analysis of oxide materials, the phase change of the active electrode materials in Na_2SO_4 electrolyte after 5000 CV cycles was also probed using Raman spectroscopy, as shown in Fig. 1b. For the as-prepared sample (Fig. 1b-1), the Raman bands at 657, 320, and 373 cm^{-1} are similar to those reported for hausmannite Mn_3O_4,[19, 20] further supporting the XRD results. For the electrode after tested for 5000 cycles (Fig. 1b-2), well-resolved Raman bands at 195, 281, 408, 480, 509, 584, and 637 cm^{-1} were observed, which are very similar to those reported for Li-birnesstie MnO_2 (280, 378, 410, 490, 510, 585, 627 cm^{-1}).[21] The general similarity of the spectral features suggest that they have a similar structure, indicating that the spinel Mn_3O_4 transformed into layered birnessite-type MnO_2 with Na^+ incorporated into the structure during electrochemical cycling in

the Na_2SO_4 electrolyte, also consisted with the XRD results.

3.2 Surface morphological study

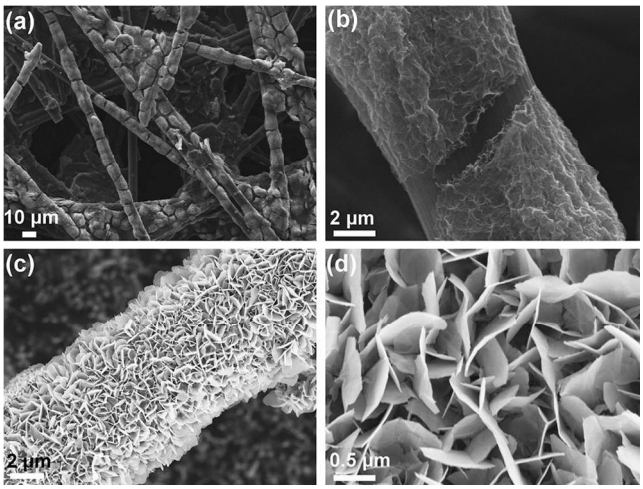

Fig. 2 (a) and (b) SEM images of the as-prepared Mn_3O_4 thin film electrode, (c) and (d) FE-SEM images of the same electrode after 5000 cycles running at a potential sweep rate of 50 mV/s.

The changes in surface morphology of Mn_3O_4 thin films after potential cycling is presented in Fig. 2. The surface view of an as-prepared Mn_3O_4 thin film appears rough but densely packed and well adhered to the substrate, as shown in Fig. 2 a and b. After 10000 CV cycles, however, the Mn_3O_4 thin film is converted to highly porous nanoflakes, as seen in Fig. 2 c and d. These porous nanoflakes would provide much larger surface area accessible for supercapacitor application. It is noted that similar surface morphology evolution of Mn_3O_4 thin film electrode was also found in previous studies.[14, 15] For instance, Dai et al.[14] reported the interlocked cube-like Mn_3O_4 thin film transformed into porous nanoflakes of birnessite MnO_2 using electrochemical cycling in aqueous Na_2SO_4.

3.3 Capacitive behaviour

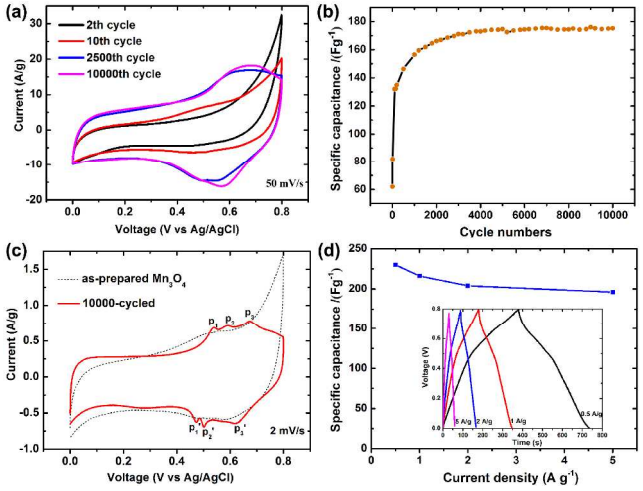

Fig. 3 Cyclic voltammograms of the sample (a) at different cycling stages, (c) before and after 10,000 cycles at a scan rate of 2 mV/s; Specific capacitance of the sample (b) as a function of cycle number at 50 mV/s, (d) at different current densities and insert shows typical charge–discharge curves of the 10,000-cycled sample at different current density.

Cyclic voltamometry (CV) was used to characterize the capacitive behaviour of the Mn_3O_4 thin film electrode in a three-electrode system with a potential ranging from 0 V to 0.8 V at a scan rate of 50 mV/s. Fig. 3a shows some typical cyclic voltammograms collected at different stages of cycling. At the second cycle, a large oxidation peak was observed toward the potential limit, indicating an irreversible oxidation of Mn_3O_4. The deviation of CV curves from a rectangle shape and low current values suggest high charge-transfer resistance and low capacitance of the Mn_3O_4 thin film electrode at the first several cycles. Subsequently, a significant increase in current is observed with cycling in the whole potential range. After 2,500 cycles, the shape of the CVs appeared more symmetric accompanied by redox peaks near 0.6 V and the current increased further even after 10,000 cycles, suggesting an increase in electrochemical reversibility and reactivity of the manganese oxide in this potential window. The specific capacitance calculated from the CV area[22] increased from 62 F g^{-1} at the second cycle to 175 F g^{-1} at the 10,000th cycle (Fig. 3b) and increased from 92 F g^{-1} to 196 F g^{-1} calculated from the discharge curve at 5 A g^{-1} (Fig. S2). Similar performance enhancement was also observed in another Mn_3O_4 sample synthesized via a hydrothermal procedure (Fig. S3). In addition, the charge-discharge rate of the 10,000-cycled sample was also characterized by chronopotentiometry at different current density, as shown in Fig. 3d. The specific capacitance (calculated from the discharge curve) of the sample was 230 F g^{-1} at 0.5 A g^{-1} and more than 85% was still remained (196 F g^{-1}) at 5 A g^{-1}, demonstrating superior rate capability (the contribution of blank carbon substrate is ignorable, Fig. S3a). To further explore the charge storage process of the manganese oxide electrode, CV profiles within the same potential window were also collected at a very slow scan rate (2 mV/s). As shown in Fig. 3c, compared with the distorted rectangular shape of as-prepared Mn_3O_4, three anodic peak centered at 0.54, 0.6 and 0.68 V and three reverse cathodic peaks centered at 0.47, 0.50 and 0.62 V were emerged in the CV curve of the 10,000-cycled electrode, which were denoted as P_1, P_2 and P_3 for anodic peaks and P_1', P_2' and P_3' for corresponding cathodic peaks (or P_{I}, P_{II} and P_{III} for the redox peak couples), respectively. These three redox peaks at different voltage may indicate that there are three different processes of cation intercalation,[16, 23] because different charge environments in the possible intercalation sites involve different conditions (e.g. voltage tension) for access and accommodation of each type of cations. The symmetry between corresponding anodic and cathodic peaks suggests that the processes of cation intercalation/deintercalation are highly reversible. The P_{I} and P_{II} peaks may be attributed to the Na^+ intercalation /deintercalation proceeded in two different sites, e.g. different vacancy sites, as reported in sodium birnessite-type manganese oxide with two intercalation sites for Li^+.[24] This is coincident with our MnO_2 thin film sample synthesized by the same electrochemical deposition procedure, but a different heat treatment at 150 ºC for 3 h in air (CV curve of the 10,000-cycled MnO_2 sample was shown in Fig. S4). While the P_3 and P_3' redox peaks are rarely reported and need careful analysis, which are likely associated with the Mn^{2+} involved redox reaction and will be discussed further in the following section. Overall, there are two types of redox reactions that involve Na^+ and Mn^{2+}, which can be expressed as follow:

$$(MnO_2^-Na^+)_{surface} - Na^+ - e^- \leftrightarrow (MnO_2)_{surface} \quad (3)$$

$$MnO_2Na_\delta - Na^+ - e^- \leftrightarrow MnO_2Na_{\delta-1} \quad (4)$$

$$(MnO_2^{2-}Mn^{2+})_{interlaminar} - e^- \leftrightarrow Mn^{3+}MnO_2^{2-} \quad (5)$$

3.4 *In operando* Raman spectroscopy studies

Since Raman spectroscopy can directly probe the near-neighbour environment of oxygen coordination around manganese and alkali cations,[19] we developed an three-compartment electrochemical system and incorporated it into our Raman microscope for *in situ* study of structural evolution of the Mn_3O_4 film during charging and discharging processes. Fig. 4c illustrates the schematic diagram of the *in situ* Raman electrochemistry experimental set-up. The electrochemical system is a simple three-electrode cell with an optical window for collecting Raman signal from the working electrode. We used low power (65 mW) of the excitation laser to minimize the potential risks of photo-induced or thermal-induced structural changes of the electrode material. An optical image of a laser spot focused on a single carbon fiber coated with active Mn_3O_4 material is shown in Fig. 4d. Fig. 4 a and b show the *in situ* Raman spectra of as-prepared Mn_3O_4 collected at different applied potentials during the CV scan at 1 mV/s. When the voltage was increased from 0 V to 1.0 V, the working electrode was positively charged, and obvious changes in Raman spectra were observed (Fig. 4a).

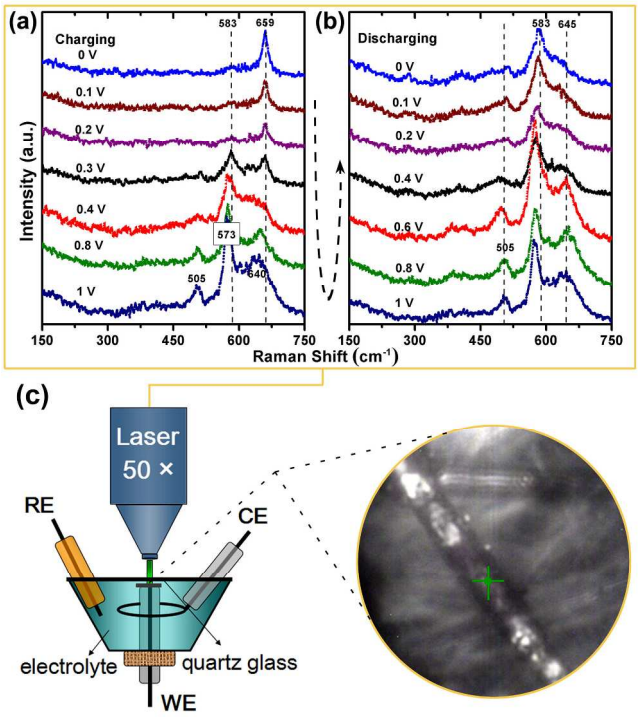

Fig. 4 *In situ* Raman spectra of the as-prepared Mn_3O_4 electrode for the initial (a) charging and (b) discharging CV cycle; The applied potential range was from 0 V to 1 V vs. Ag/AgCl with a scan rate of 1 mV/s. (c) Scheme of *in-situ* Raman electrochemistry experimental configuration and an optical image of a laser spot on a single carbon fiber coated with a uniform coating of active material.

At 0 V, only a sharp band at 659 cm^{-1} was observed, which is the characteristic band of Mn_3O_4 spinel structure. This peak is assigned to the A_{1g} mode and corresponds to the Mn-O breathing vibration of Mn^{2+} in tetrahedral coordination.[19] As the potential increased to 0.3 V, the 659 cm^{-1} band became weaken in intensity, as well as two new bands at about 583 cm^{-1} and 505 cm^{-1} emerged. This suggests that a new structural phase appeared, indicating the beginning of phase transition of Mn_3O_4 under applied potential. While from 0.4 V to 1.0 V, a wide band at about 640 cm^{-1} began to appear and gradually became stronger in intensity and the band at 659 cm^{-1} disappeared. And the new emerged bands experienced a shift along with the potential rise, e.g. 583 to 573 cm^{-1}. It is noted that these three new bands are in good agreement with the values (646, 575 and 506 cm^{-1}) reported for birnessite MnO_2 ($MnO_{1.86}{\cdot}0.6H_2O$),[25] which includes a mixture of Mn (IV) and Mn (II) and has a trigonal structure comprising of non-superimposed octahedra [MnO_6] sheets. The peak at 575 cm^{-1} is usually assigned to the (Mn-O) stretching vibration in the basal plane of [MnO_6] laminates, which is particularly related to the rate of Mn (IV) in birnessite compounds. These Raman signal changes indicate that the initial spinel Mn_3O_4 was transformed to a layered birnessite MnO_2 during the charging process. While during the discharging process from 1 V to 0 V, the bands at 645, 573, and 507 cm^{-1} became weaker and broader, whereas the main band at 573 cm^{-1} was shifted to 583 cm^{-1}, corresponding likely to the intercalation of cations between the laminates of birnessite MnO_2. From these *in situ* Raman results, it can be seen that the phase transition of Mn_3O_4 to birnessite-type MnO_2 is completed when the potential is increased to 0.4 V and this process is irreversible in our three electrode configuration at a very slow sweep rate, which appears to be different from our prior report.[17] The difference should be originated from the different initial structure of active material and the concentration of Mn^{2+} in the electrolyte. Moreover, the phase change from Mn_3O_4 to birnessite-type MnO_2 could be the structural origin of the increase in the conductivity and capacitance of the sample after cycling. In addition, it should be noted that, at a higher scan rate of 50 mV/s, it would take thousands CV cycles to enable all of the Mn_3O_4 transform into birnessite MnO_2 completely, corresponding to the slow increase of anodic and cathodic currents upon potential cycling (Fig. 3a).

To further uncover the charge storage behavior of the transformed birnessite MnO_2 during potential cycling, *in situ* Raman measurements were also employed to examine the samples (birnessite MnO_2, $MnO_{1.86}{\cdot}0.6H_2O$) after being cycled for 10,000 cycles at a scan rate of 50 mV/s. Fig. 5 shows the Raman spectra collected at different potentials separated by 0.1 V. As usual, the *in situ* CV test was performed at a scan rate of 1 mV/s within the potential range from 0 V to 1 V. Three major Raman bands associated with energy storage process were observed at 625-658 (v_1), 574-586 (v_2), and 280 cm^{-1} (v_3); all exhibited reversible evolution during the charging and discharging process. The v_2 band was shifted to lower wavenumber (from 585 to 574 cm^{-1}) when the applied voltage was increased from 0 V to 1 V and then shifted back to 586 cm^{-1} as the voltage dropped to 0 V. During the charging process, the decrease in wavenumber for the Mn-O stretching mode was caused by the lattice softening that corresponds to the expansion of the [MnO_6] laminates because of the gradually revealed laminar electrostatic repulsion after the extraction of Na^+ and the introduce of water molecules.

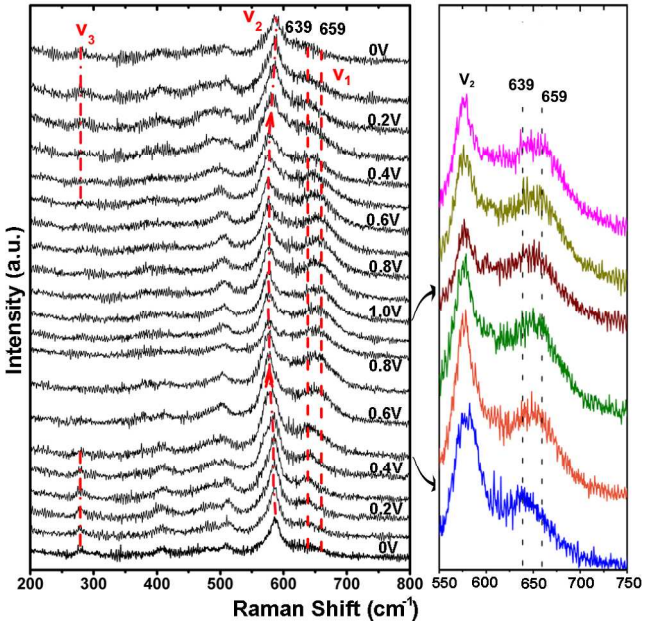

Fig. 5 *In situ* Raman spectra of the transformed birnessite-type MnO_2 collected at different potentials separated by 0.1 V in 1 M Na_2SO_4.

Accordingly, the ν_3 Raman band at 280 cm^{-1}, attributed to the weak bonding of the intercalated electrolyte cations (Na^+) between the [MnO_6] laminates,[21] gradually weakened until disappeared at the charging process because of the extraction of Na^+ and experienced an opposite change when discharged. The ν_1 band at 638 cm^{-1} became broader and a clear shoulder band centered at about 659 cm^{-1} emerged when the potential was increased to 0.7 V, corresponding to the partial oxidation of Mn^{2+} (distributed between the [MnO_6] laminates) to Mn^{3+} and hence the emergence of some Mn_3O_4 after the deintercalation of Na^+. This reaction was reversible and Mn^{3+} was reduced back to Mn^{2+} at the discharging process. The potential value (about 0.7V) at which 659 cm^{-1} band emerged is almost the same as that when P_3 peak emerged in the CV curve of Fig. 3c, further confirming the Mn^{2+} involved energy storage behaviour described in equation (5). The detailed wavenumber changes of these Raman bands upon potential cycling were illustrated in Fig. S5. To further verify the influence of Mn^{2+}, some additional Mn^{2+} was added into the electrolyte, and we found that the Raman signal attributed to MnO_2 drastically changed into that of Mn_3O_4 (Fig. S6), which suggested an important role of Mn^{2+} in the energy storage process.

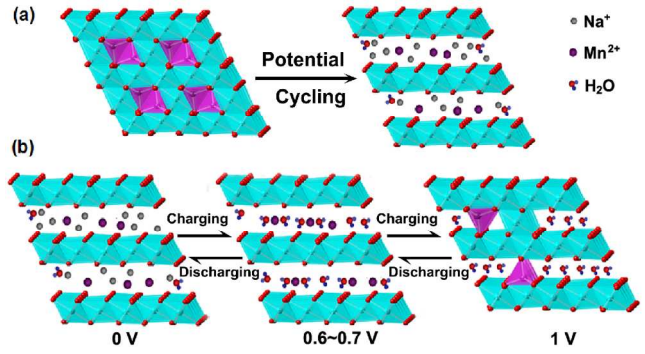

Fig.6 Phase transformation during the charging/discharging process speculated from the *in situ* Raman results.

The above *in situ* Raman results imply that two types of redox reactions contributed to the energy storage of transformed birnessite MnO_2, including the intercalation/deintercalation of Na^+ and oxidation/reduction of Mn^{2+}, which is quite consistent with the CV profile acquired at low scan rates. In additional, there are no observable spectral features that suggest intercalation/deintercalation of H^+ in the active electrode materials because there are no bands assigned to the middle phase MnOOH which is very sensitive to Raman. Although the capacitance of the active materials studied is not very high (230 F g^{-1} at 0.5 A g^{-1}), the purpose of this study is to gain insights into the mechanism of charge storage in the active electrode materials.

On the basis of these *in situ* Raman studies and the corresponding electrochemical measurements, the phase transformation processes associated with the energy storage process are schematically illustrated in Fig. 6. The nano-structured Mn_3O_4 prepared at relative low temperatures is not stable under potential cycling. It was transformed to a laminar birnessite-type MnO_2 with Na^+ and Mn^{2+} filled in the defect sites or between the laminates initially at the first few cycles. At positive scan, Mn^{2+} cations were extracted from the tetrahedral sites whereas the Mn^{3+} cations located at the same layer can be reduced to Mn^{2+} during the negative scan. Gradually, more stable birnessite-type MnO_2 with Na^+ and Mn^{2+} filling was formed, which store/release energy through intercalation/deintercalation of Na^+ as well as oxidation/reduction of Mn^{2+}.

Conclusion

In summary, a detailed structural evolution of Mn_3O_4 as pseudo-capacitor electrode upon potential cycling was investigated systematically using *ex situ* and *in operando* Raman spectroscopy. The *in operando* Raman investigations revealed that the spinel Mn_3O_4 are susceptible to the applied potential and can transform into birnessite-type MnO_2 during potential cycling in a Na_2SO_4 electrolyte via the extraction of Mn^{2+} cations, which is the main reason for the much improved electrochemical performance along with cycling. The phase transformation can be realized in relative early stage of the first cycle (before the applied potential increased to 0.4 V) when the scan rate is relatively slow (1 mV/s), allowing full reaction of the active materials. A directly crystal structure change induced by the extraction of Mn^{2+} cations was proposed in this phase transition process. Additionally, the energy storage behavior of transformed birnessite MnO_2 was also carefully studied. It was found that the newly generated birnessite MnO_2 with Na^+ and Mn^{2+} filling in the defect sites (or between the laminates) experienced a reversible structure change corresponding to the intercalation/deintercalation of Na^+ and the oxidation/reduction of Mn^{2+} during potential cycling. However, there were no observable Raman spectral features that suggest the involvement of H^+ in the energy storage process, which implies that the traditional energy storage reactions is not suitable to every Mn-based oxide, a little bit different in different crystal structures. This could be the main reason that our samples have such good cycling life, which is comparable to carbon based electrodes. It is hoped that these results and the gain fundamental understanding may guide us to achieve rational design of more efficient manganese oxides based electrode materials for high performance

supercapacitors.

Acknowledgement

The research was supported by the "Outstanding Talent and Team Plans Program" of South China University of Technology (SCUT), the National Science Foundation for Young Scientists of China (No. 21403073) and Fundamental Research Funds for Central Universities of SCUT, China (No. 2013ZM058), Chinese National Natural Science Foundation (No. 11474101).

Notes and references

[a] *New Energy Research Institute, School of Environment and Energy, South China University of Technology, Guangzhou Higher Education Mega Center, Guangzhou, Guangdong 510006, China.*
[*] *E-mail: escheng@scut.edu.cn, Tel: 86+020+39380525.*
[b] *School of Materials Science and Engineering, Georgia Institute of Technology, 771 Ferst Drive, Atlanta, GA 30332-0245, USA.*
[*] *E-mail: meilin.liu@mse.gatech.edu, Tel: 404-894-6114.*
[c] *State Key Laboratory of Optoelectronic Materials and Technologies, School of Physics and Engineering, Sun Yat-sen University, Guangzhou 510275, China*

1. A. Burke, CrossRef, CAS, Web of Science® Times Cited, 856.
2. B. E. Conway, *Scientific Fundamentals and Technological Applications*, Kluwer Academic/Plenum Publishers, New York. (1999).
3. J. Chmiola, G. Yushin, Y. Gogotsi, C. Portet, P. Simon and P.-L. Taberna, *Science*, 2006, 313, 1760-1763.
4. P. Simon and Y. Gogotsi, *Nat. Mater.*, 2008, 7, 845-854.
5. P. J. Hall, M. Mirzaeian, S. I. Fletcher, F. B. Sillars, A. J. Rennie, G. O. Shitta-Bey, G. Wilson, A. Cruden and R. Carter, *Energy Environ. Sci*., 2010, 3, 1238-1251.
6. C. Lin, B. N. Popov and H. J. Ploehn, *J. Electrochem. Soc.*, 2002, 149, A167-A175.
7. G. A. Snook, P. Kao and A. S. Best, *J. Power Sources*, 2011, 196, 1-12.
8. M.-K. Song, S. Cheng, H. Chen, W. Qin, K.-W. Nam, S. Xu, X.-Q. Yang, A. Bongiorno, J. Lee and J. Bai, *Nano Lett.*, 2012, 12, 3483-3490.
9. L. Huang, D. Chen, Y. Ding, S. Feng, Z. L. Wang and M. Liu, *Nano Lett.*, 2013, 13, 3135-3139.
10. H. JináFan, *Energy Environ. Sci*., 2011, 4, 4496-4499.
11. T. Brousse, M. Toupin, R. Dugas, L. Athouël, O. Crosnier and D. Bélanger, *J. Electrochem. Soc.*, 2006, 153, A2171-A2180.
12. D. J. Jones, E. Wortham, J. Rozière, F. Favier, J.-L. Pascal and L. Monconduit, *J. Phys. Chem. Solids*, 2004, 65, 235-239.
13. Y. Lei, C. Fournier, J.-L. Pascal and F. Favier, *Micropor.Mesopor.Mat.*, 2008, 110, 167-176.
14. D. P. Dubal, D. S. Dhawale, R. R. Salunkhe and C. D. Lokhande, *J. Electrochem. Soc.*, 2010, 157, A812-A817.
15. D. Dubal, D. Dhawale, R. Salunkhe and C. Lokhande, *J. Electroanal. Chem.*, 2010, 647, 60-65.
16. L. Athouël, F. Moser, R. Dugas, O. Crosnier, D. Bélanger and T. Brousse, *J. Phys. Chem. C*, 2008, 112, 7270-7277.
17. S. Cheng, L. Yang, D. Chen, X. Ji, Z. Jiang, D. Ding and M. Liu, *Nano Energy*, 2014, 9, 161-167.
18. S. Fritsch, J. Sarrias, A. Rousset and G. Kulkarni, *Mater. Res. Bull.*, 1998, 33, 1185-1194.
19. C. Julien, M. Massot and C. Poinsignon, *Spectrochimica Acta Part A: Molecular and Biomolecular Spectroscopy*, 2004, 60, 689-700.
20. B. R. Strohmeier and D. M. Hercules, *J. Phys. Chem.*, 1984, 88, 4922-4929.
21. C. Julien, M. Massot, R. Baddour-Hadjean, S. Franger, S. Bach and J. Pereira-Ramos, *Solid State Ionics*, 2003, 159, 345-356.
22. C. Xu, H. Du, B. Li, F. Kang and Y. Zeng, *J. Electrochem. Soc.*, 2009, 156, A435-A441.
23. A. l. Boisset, L. Athouël, J. Jacquemin, P. Porion, T. Brousse and M. r. m. Anouti, *J. Phys. Chem. C*, 2013, 117, 7408-7422.
24. Q. Feng, H. Kanoh, Y. Miyai and K. Ooi, *Chem. Mater.*, 1995, 7, 1226-1232.
25. S. Bach, J.-P. Pereira-Ramos, C. Cachet, M. Bode and L. T. Yu, *Electrochim. Acta*, 1995, 40, 785-789.

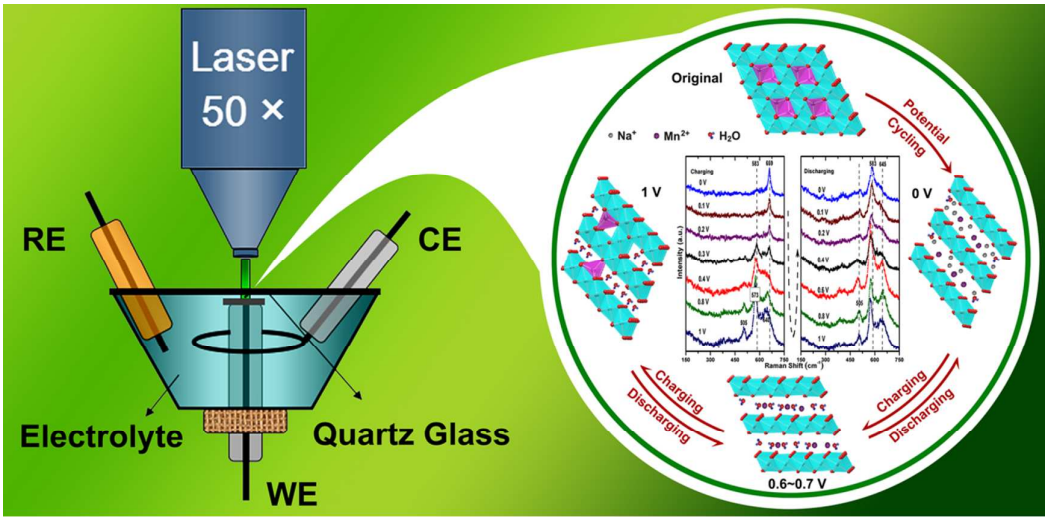

In *operado* Raman spectroscopy were used to monitor the origin of pseudocapacitive behavior of Mn_3O_4 electrodes during charging/discharging processes.